Supplementary Information:

Rapid Perovskite Formation by CH_3NH_2 Gas-Induced Intercalation and Reaction of PbI_2

Sonia R. Raga[1,†], Luis K. Ono[1,†], Yabing Qi[1]*

[1]Energy Materials and Surface Sciences Unit (EMSS), Okinawa Institute of Science and Technology Graduate University (OIST), 1919-1 Tancha, Onna-son, Kunigami-gun, Okinawa 904-0495, Japan.

*Corresponding author. E-mail: Yabing.Qi@OIST.jp

[†]These authors contributed equally to this work.

Content:

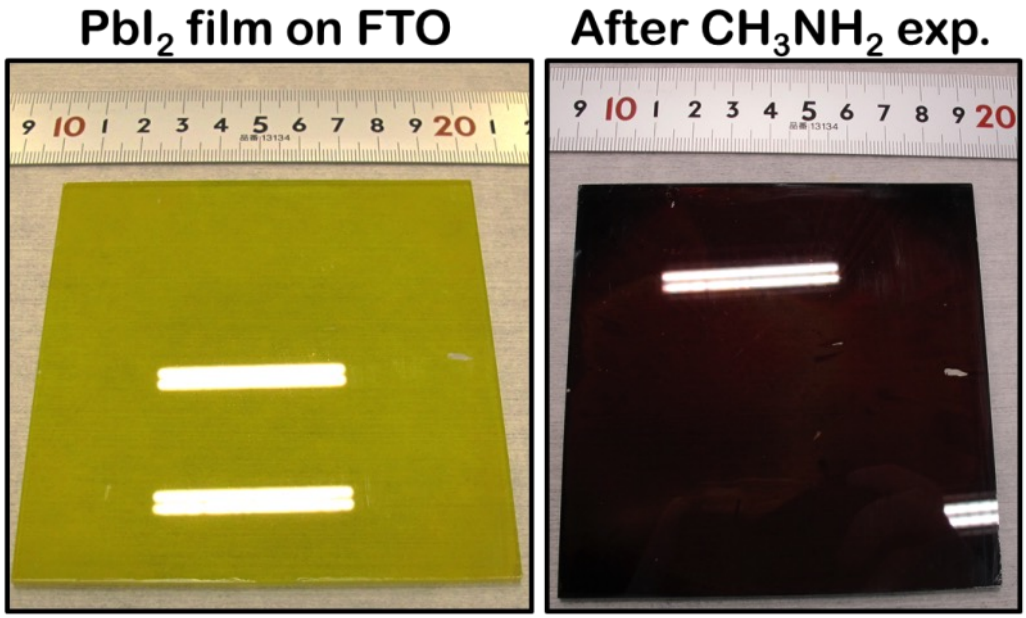

Figure S1. Demonstration of the large area processing of the MA step. A PbI_2 film on a 10 x 10 cm^2 FTO substrate exposed to CH_3NH_2 gas. The technique can be easily adapted for perovskite fabrication on large-area substrates, with complete conversion at room temperature and in a short time scale (within ~1 min).

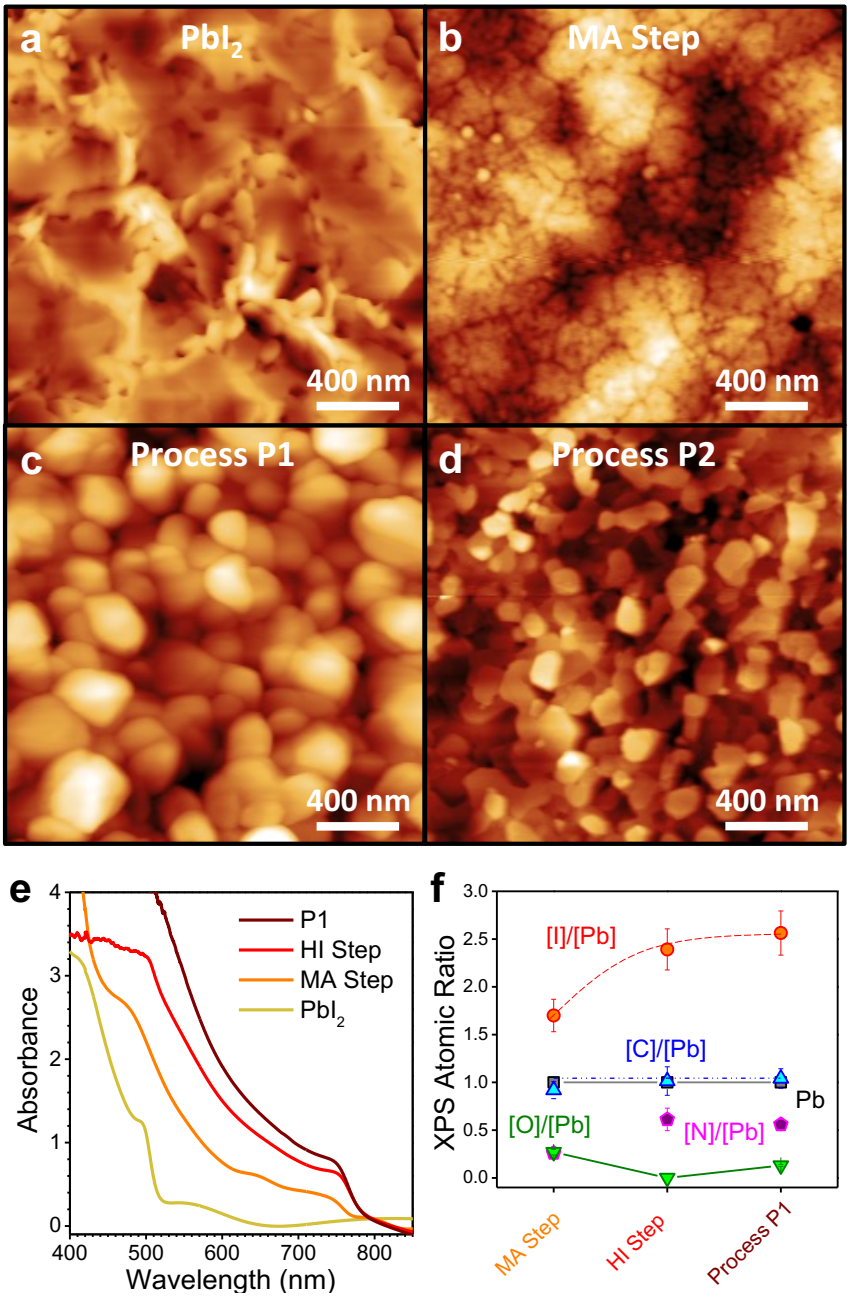

Figure S2. Morphological characterization of perovskites formed by methylamine and hydroiodic gas exposures. a-d, Tapping-mode AFM images of the spin-coated PbI_2 film (**a**) and the film with subsequently treatment of the MA step (**b**), Process P1 (**c**), and Process P2 (**d**). The formation of large crystallites with ~400 nm grain sizes can be observed after Process P1 (2 cycles). The corresponding RMS values extracted from the AFM images: 21 nm (PbI_2), 2 nm (MA step), 14 nm (Process P1), and 6 nm (Process P2). **e,f**, UV-vis (**e**) and XPS atomic ratios (**f**) monitored after each of the described processes.

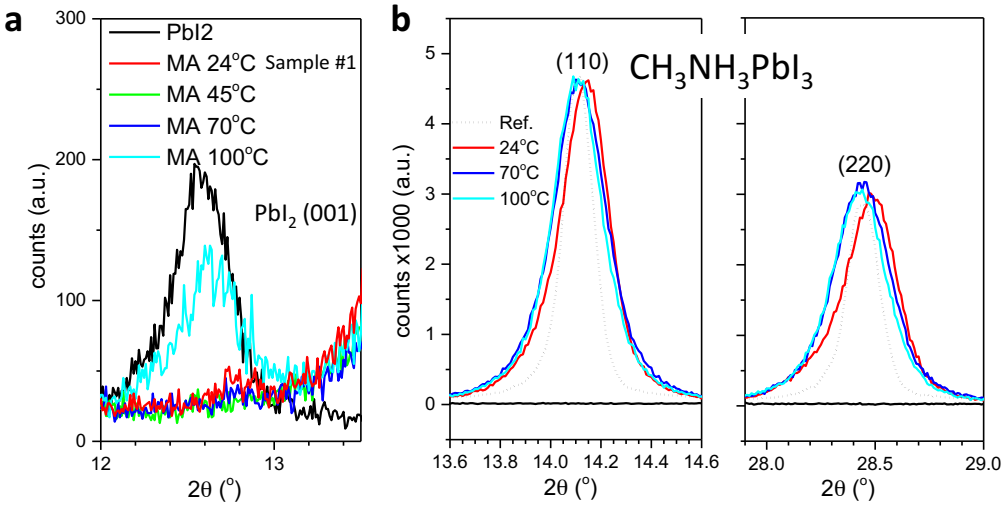

Figure S3. Study of the MA step followed by the post-annealing treatment. XRD peaks corresponding to **a,** PbI_2 (001) and **b,** $CH_3NH_3PbI_3$ perovskite (110) and (220) peaks. Samples #1 were formed at 24°C and followed by the post-annealing treatment at different temperatures (45, 70, and 100°C). XRD peaks corresponding to the perovskite sample synthesized by the conventional method from PbI_2 and CH_3NH_3I precursors are shown for comparison (labelled as Ref). All Samples #1 with or without the post-annealing treatment showed much broader peak width than the reference perovskite sample. This observation can be explained by the smaller crystal sizes obtained on Sample #1 in comparison to the reference sample.

We investigated systematically the MA step process followed by an immediate post-annealing step aiming at the formation of films with higher crystallinity **(Supplementary Fig. S3**). The XRD (110) peak position (2θ) and peak broadening (full width at half maximum, FWHM) on perovskite films prepared by MA step (Sample #1) with different post-annealing temperatures (45°C, 70°C, and 100°C) and by the standard one-step solution-processing using CH_3NH_3I and PbI_2 precursors, Ref. sample, were compared[1]. The Ref.

sample revealed the formation of large crystal grain, which induced the narrowest peak width in XRD **(Supplementary Fig. S3)**. All the perovskites formed by the MA step resulted in much broader peak widths corroborating with the AFM results on the smaller grain sizes, **Supplementary Fig. S2b**. Interestingly, a slight XRD (110) peak shift on Samples #1 at 24°C (2θ = 14.15°) and compared to the Ref. sample (2θ = 14.11°) was observed. The instrumental diffraction angle resolution is 0.01°. According to Bragg's law, it corresponded to a lattice constant contraction of about 0.3%. When performing the post-annealing treatment on Samples #1 at 70°C or 100°C, the (110) XRD peaks went back to the reference value (14.11°). Based on the previous reports, assuming the presence of iodine vacancies of V_I ~8.3%, volume contraction of ~11% (i.e. one-dimensional contraction of ~3.8%) was calculated considering the case of perovskite with cubic structure[2]. Therefore, our XRD measurements indicate that the perovskite crystals formed by the MA step did not generate appreciable number of defects, i.e., the major $CH_3NH_3PbI_3$ formed as a result of MA step is in *stoichiometric* form.

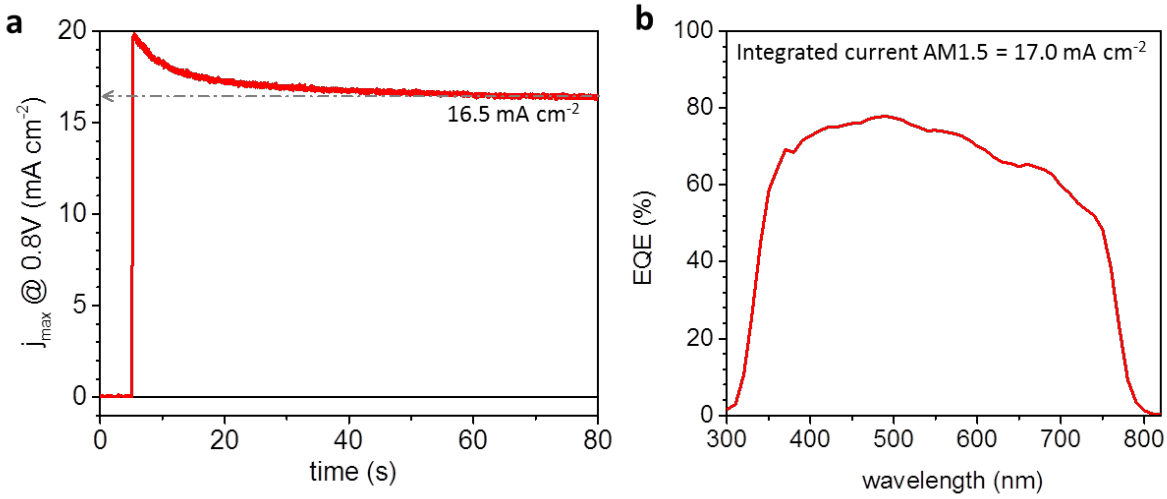

Figure S4. Steady state current measurement. a, The cell was illuminated under 1 sun, and after ~5 s the circuit was closed under the bias voltage of 0.8 V, which corresponded to the cell maximum power point. The steady state current is approximately 16.5 mA/cm^2. **b**, External quantum efficiency (EQE) measured at an interval of 10 nm. The integrated current for AM1.5 illumination is approximately 17.0 mA cm^{-2}.

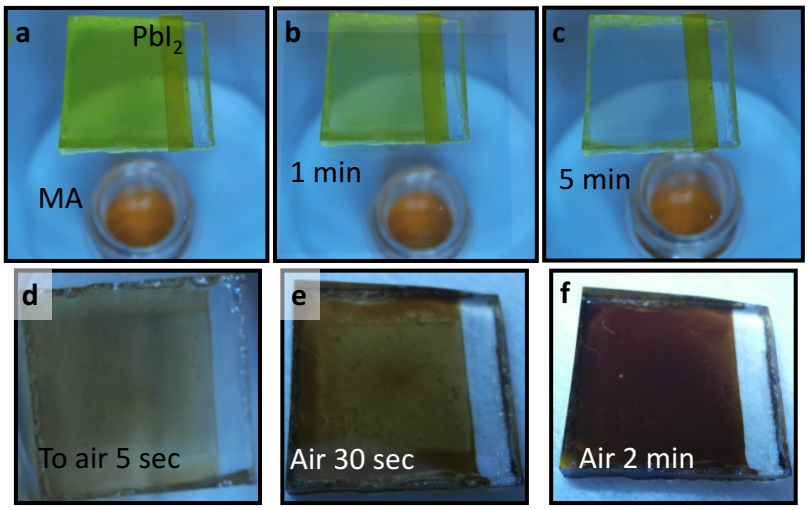

Figure S5. PbI_2 exposure to CH_3NH_2 gas in dry atmosphere. Images of a PbI_2 film **a,** deposited on mesoporous TiO_2 and subsequent exposed to MA gas inside the N_2 glovebox (< 0.1ppm H_2O) after **b,** 1 min and **c,** 5 min. The film was removed from MA exposure and retained a pale-yellow color. It was then transferred out of the glovebox to air, and the film immediately started turning **d,** brown in color. Prolonged air exposure led to the further darkening of the film color: **e,** 30 s and **f,** 2 min.

The interaction between PbI_2 and MA in the absence of H_2O was studied in a dry environment such as in a N_2 glovebox with H_2O levels below 0.1 ppm **(Supplementary Fig. S5a,b,c)**. No perovskite formation was observed after the MA step in the N_2 glovebox. The initial yellow PbI_2 film turned transparent with gradual MA exposure **(Supplementary Fig. S5c)**. Similar color change of PbI_2 from yellow to white after MA exposure has been observed previously in inert atmosphere[3]. However, when these films were taken out from the N_2 glovebox to ambient air (RH ~ 50%), we observed the color change to dark red/brown immediately **(Supplementary Fig. S5d,e,f)** indicating the $CH_3NH_3PbI_3$ perovskite formation,

which was further confirmed by UV-vis and XRD measurements (data not shown). The similar process has been observed previously in chemical vapor deposition techniques[4].

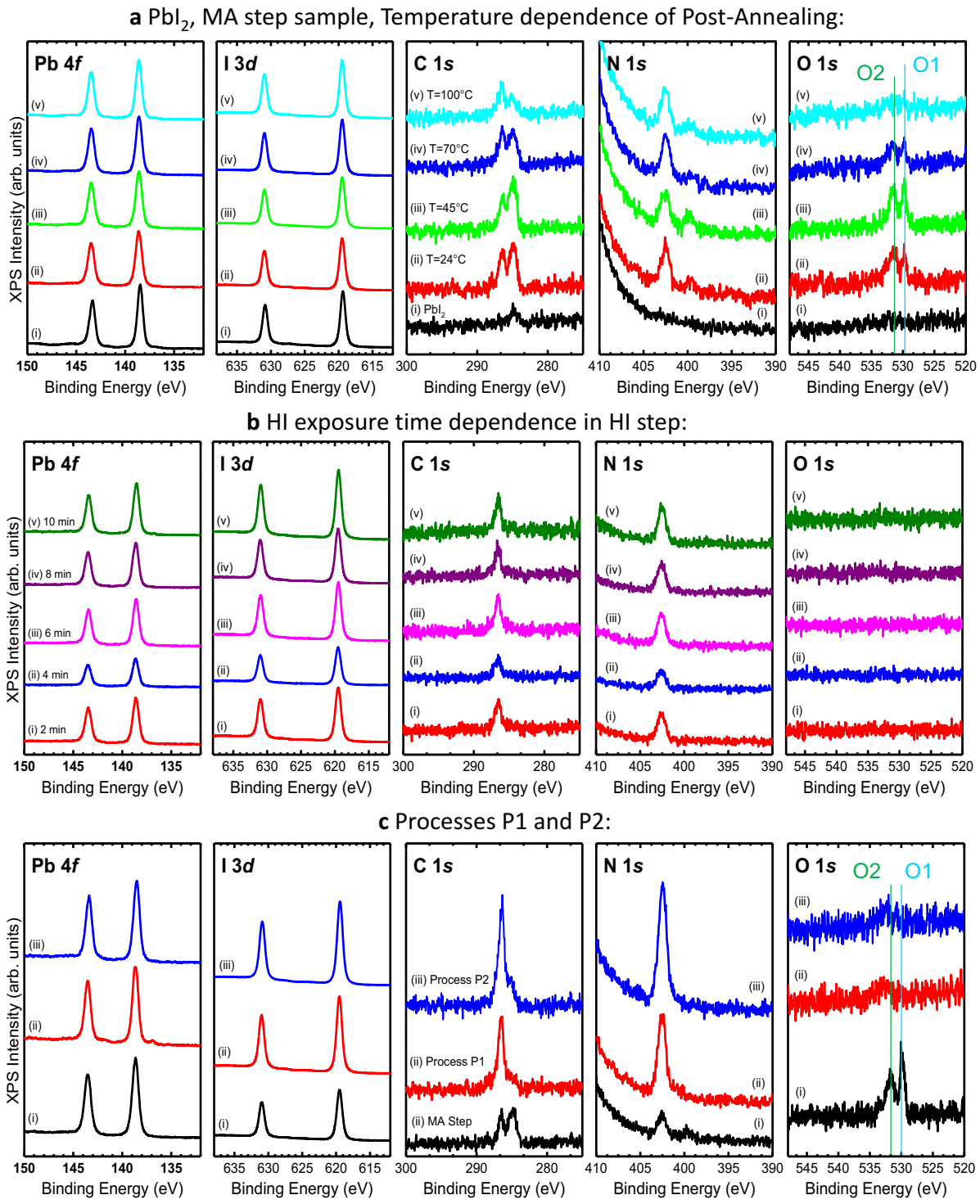

Figure S6. Chemical composition analysis by XPS of methylamine and hydroiodic acid gas induced perovskite. XPS spectra (Al-Kα=1486.6 eV) corresponding to Pb 4*f*, I 3*d*, C 1*s*, N 1*s*, and O 1*s* core levels of PbI_2 films processed by exposure to MA and HI gases. **a, the** MA step followed by subsequent substrate annealing at different temperatures (45°C to

100°C) for 3 min. **b,** the HI step performed with different times (2 min to 10 min). **c,** Sample (after the MA step) before and after two cycles of HI exposure for 2 min followed by the MA exposure for 4 min (Processes P1 and P2).

The single peak position of Pb $4f_{7/2}$ (138.7 eV) in our studies matched well with Pb in the 2+ oxidation state [5]. Therefore, the different Pb^{2+}-related compounds were observed to overlap. For example, PbI_2 and $PbO/Pb_xO_y/Pb(OH)_2$ compounds were previously reported to show Pb $4f_{7/2}$ peaks in the binding energy (BE) ranges of 138.4–138.9 eV and 137.6–138.4 eV, respectively[5-8]. The range of BE reported for $CH_3NH_3PbI_3$ perovskite is 138.5–138.8 eV[9,10]. Similar to Pb 4*f* region, the single I $3d_{5/2}$ BE value (619.5 eV) observed for the samples with different MA and HI treatments matched well with several compounds reported in literature. For example, I $3d_{5/2}$ in PbI_2 was reported to be in the range of 619.4–619.5 eV[5,6]. For $CH_3NH_3PbI_3$ perovskite the BE values of I $3d_{5/2}$ are in the range of 619.5–619.6 eV[9,10]. The metallic Pb signal, with the expected Pb $4f_{7/2}$ peak in the range of 136.6–137 eV, was below the instrument detection limit, indicating good resistance of the films to beam damage within XPS measurement time[9,10]. Two chemical states were observed in C 1*s* (286.6 eV and 284.9 eV) and N 1*s* (399.6 eV and 402.6 eV) core levels after the MA step **(Supplementary Fig. S6a)**. The C 1*s* and N 1*s* peaks at higher BEs of 286.6 eV and 402.6 eV, respectively, were correlated with the incorporation of $CH_3NH_3^+$ in perovskite[10,11]. The C 1*s* and N 1*s* components at lower BEs 284.9 eV and 399.6 eV, respectively, were present only in Samples #1 and these peaks disappear after the subsequent HI exposure. At the moment, the assignments of the lower BE C 1*s* and N 1*s* components are not clearly understood and is under further investigation in our laboratory.

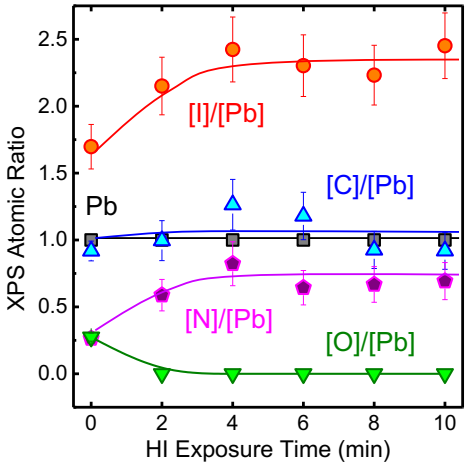

Figure S7. Time dependence of the HI step. Surface [I,C,N,O]:[Pb] atomic ratio extracted by integrating the XPS peak areas on the samples after the MA step (0 min) followed by the HI step with different HI exposure times (2–10 min).

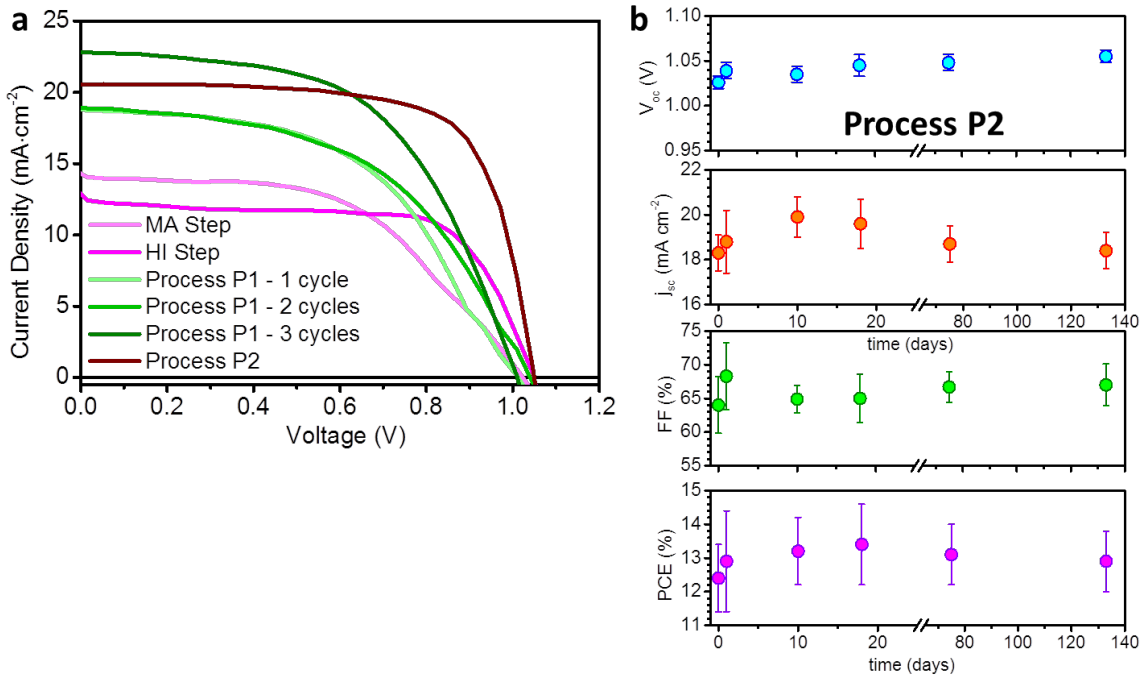

Figure S8. *j-V* curves for the samples with the best efficiencies from all batches and the stability of Process P2 devices. a, *j-V* curves corresponding to the PbI_2 film after the MA step (light pink curve); The MA step sample exposed to HI gas for 3 min (HI step, dark pink curve); The MA step samples exposed to 1, 2, and 3 cycles of sequential exposure to HI gas for 2 min and MA gas 4 min (Process P1, green curves); and the MA step samples exposed simultaneously to MA and HI gases for 10 min at 70°C (Process P2, brown curve). **b,** Stability profile of solar cell devices fabricated following Process P2. Evolution of solar cell performance parameters, i.e., open circuit voltage (V_{oc}), short circuit current (j_{sc}), fill factor (FF), and power conversion efficiency (PCE) over 133 days of storage in a N_2 glovebox under a low illumination condition.

Table S1. Photovoltaic parameters corresponding to the solar cells in **Supplementary Figure S8**.

	V_{oc} (V)	j_{sc} (mA cm^{-2})	*FF* (%)	PCE (%)
MA Step	1.022	14.2	52.2	7.6
HI Step	1.049	12.5	68.3	8.9
Process P1 - 1cycle	1.010	18.8	51.4	9.7
Process P1 – 2 cycles	1.033	18.9	51.2	10.0
Process P1 – 3 cycles	1.010	22.8	55.6	12.7
Process P2	1.049	20.6	70.8	15.3

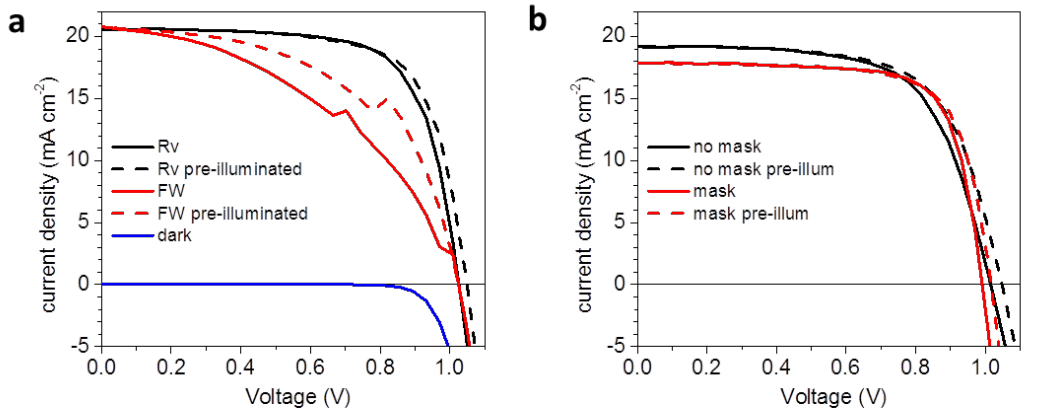

	V_{oc} (V)	J_{sc} (mA cm^{-2})	FF (%)	PCE (%)
RV	1.026	20.6	70.8	15.0
RV pre-illum	1.049	20.6	70.8	15.3
FW	1.016	20.7	46.9	9.9
FW pre-illum	1.024	20.8	57.4	12.2

	V_{oc} (V)	J_{sc} (mA cm^{-2})	FF (%)	PCE (%)
No mask	1.016	19.2	65.4	12.7
No mask pre illum	1.048	19.2	65.9	13.3
Mask	0.991	17.9	73.8	13.1
Mask pre illum	1.017	17.9	72.2	13.1

Figure S9. Effects of the hysteresis and masking on the solar cell efficiencies. a, *j-V* curves corresponding to a sample prepared by Process P2 measured at 0.1V/s from 1.2V → 0V (black line) with pre-illumination of 5 s (dashed black line), and from 0V → 1.2V (red line) with pre-illumination of 5 s (dashed red line). The same sample measured in dark (blue line). **b,** *j-V* curves corresponding to a P2 sample measured 18 days after fabrication with and without a mask during measurements. The area of the device was 0.09 cm^2 and the area of the mask 0.04 cm^2. The effects of pre-illumination of 5 s are also shown (dashed lines). The j_{sc} reduction by the effects of mask is compensated by an improvement in FF, leading to a similar PCE. The detailed photovoltaic parameters of each curve are shown in the table below the corresponding plot.

References:

1 Zhou, H. *et al.* Interface engineering of highly efficient perovskite solar cells. *Science* **345**, 542-546 (2014).

2 Azpiroz, J. M., Mosconi, E., Bisquert, J. & De Angelis, F. Defect migration in methylammonium lead iodide and its role in perovskite solar cell operation. *Energy Environ. Sci.* **8**, 2118-2127 (2015).

3 Warren, R. F. & Liang, W. Y. Raman spectroscopy of new lead iodide intercalation compounds. *J. Phys. Condens. Matter* **5**, 6407-6418 (1993).

4 Leyden, M. R., Lee, M. V., Raga, S. R. & Qi, Y. B. Large formamidinium lead trihalide perovskite solar cells using chemical vapor deposition with high reproducibility and tunable chlorine concentrations. *J. Mater. Chem. A* **3**, 16097-16103 (2015).

5 *X-ray Photoelectron Spectroscopy Database, Version 3.4 (Web Version), http://srdata.nist.gov/xps/index.htm*.

6 Zheng, Z. *et al.* In situ growth of epitaxial lead iodide films composed of hexagonal single crystals. *J. Mater. Chem.* **15**, 4555-4559 (2005).

7 Jo, C. H. *et al.* Low-temperature annealed PbS quantum dot films for scalable and flexible ambipolar thin-film-transistors and circuits. *J. Mater. Chem. C* **2**, 10305-10311 (2014).

8 Luther, J. M. *et al.* Structural, optical, and electrical properties of self-assembled films of PbSe nanocrystals treated with 1,2-ethanedithiol. *ACS Nano* **2**, 271-280 (2008).

9 Lindblad, R. *et al.* Electronic structure of $TiO_2/CH_3NH_3PbI_3$ perovskite solar cell interfaces. *J. Phys. Chem. Lett.* **5**, 648-653 (2014).

10 Raga, S. R. *et al.* Influence of air annealing on high efficiency planar structure perovskite solar cells. *Chem. Mater.* **27**, 1597-1603 (2015).

11 Yan, J., Ke, X., Chen, Y., Zhang, A. & Zhang, B. Effect of modulating the molar ratio of organic to inorganic content on morphology, optical absorption and photoluminescence of perovskite $CH_3NH_3PbBr_3$ films. *Appl. Surf. Sci.* **351**, 1191-1196 (2015).